

Superconductivity in SrTiO₃: dielectric function method for non-parabolic bands

S. N. Klimin, J. Tempere,* and J. T. Devreese
*Theorie van Kwantsystemen en Complexe Systemen (TQC),
Universiteit Antwerpen, Universiteitsplein 1, B-2610 Antwerpen, Belgium*

J. He, C. Franchini, and G. Kresse
Faculty of Physics, Computational Materials Physics, University of Vienna, Vienna A-1090, Austria
(Dated: November 29, 2018)

The dielectric function method for superconductivity has been applied to SrTiO₃ accounting for the non-parabolic dispersion of charge carriers in the conduction band and for the dispersion of optical phonons based on density functional theory calculations. The obtained critical temperatures of the superconducting phase transition in SrTiO₃ are in agreement with experiments in the density range $n \sim 5 \times 10^{18}$ to 5×10^{20} cm⁻³. The dielectric function method predicts also the sign of the anomalous isotope effect in strontium titanate, in line with recent observations.

INTRODUCTION

Superconductivity in SrTiO₃, discovered a long time ago [1–3] attracts a renewed experimental [4–9] and theoretical [9–16] interest because strontium titanate exhibits the superconducting transition at very low carrier densities.

Different physical mechanisms are considered to explain superconductivity in SrTiO₃, e. g., dynamically screened electron-LO-phonon interactions [9–13], interaction of electrons with quantum ferroelectric fluctuations [14], with the soft TO-phonon mode [15] and with local phonons [16]. All these studies are in line with experiments. Nevertheless, the physical picture of superconductivity in SrTiO₃ is still far from clarity.

Besides physical mechanisms, the key question concerns the method. Migdal-Eliashberg theory [17] is hardly applicable here, because the energies of LO phonons in doped SrTiO₃ are comparable with the Fermi energy of electrons at typical concentrations relevant for the experiments. Nevertheless, this standard approach of superconductivity is exploited in recent works [10, 16]. A generalization of the BCS theory beyond the adiabatic regime was derived by Kirzhnits, Maksimov and Khomskii (KMK) [18] who described the electron-phonon and Coulomb interactions through the dielectric function.

As a downside of this generalization, the dielectric function method (DFM) developed by KMK is a weak-coupling approach. The electron-phonon coupling in strontium titanate is not weak [19], especially at low concentrations. Consequently, the DFM can be uncontrolled, especially at low densities (where the electron-phonon interaction is stronger) and not able to obtain quantitatively accurate results for SrTiO₃. However it can give a qualitatively correct picture of

the concentration-dependent superconducting transition temperature [9, 12, 13, 22]. A verification of the KMK ansatz within the non-adiabatic extension of the Eliashberg theory [11] showed compatibility of these two methods.

The present work does not claim to explain all aspects of superconductivity in SrTiO₃, because the picture seems to be more complicated than can what be described by a unique mechanism for all concentrations. We restrict the treatment to only the most usual interactions which are definitely present in SrTiO₃: the electron-phonon interaction with LO and acoustic phonons, and the Coulomb repulsion. The DFM with these interactions seems to be applicable for SrTiO₃ except at very low densities $n \lesssim 10^{18}$ cm⁻³, where the experiment [4] reveals a separate superconducting dome which correlates with the evolution of the Fermi surface with doping [20].

In Refs. [9, 15], experimental data on the transition temperature have been reasonably explained using, respectively, DFM and the Morel-Anderson theory [21] in the effective mass approximation, and including in Ref. [15] the deformation potential interaction with the soft TO-phonon mode. In the present work, we apply the extension of the DFM for a non-parabolic band structure and incorporate the interaction with acoustic phonons. It is interesting that the softening of the lowest TO-phonon mode influences the dielectric function and hence enhances T_c even before introducing the deformational electron – TO-phonon interaction. The other new element is a multimode dielectric function different from that used in Ref. [22] and accounting for non-parabolic phonon dispersion. We analyze also the anomalous isotope effect in SrTiO₃ [23].

THEORETICAL DESCRIPTION

In this section, DFM is revisited taking into account non-parabolicity of the conduction band. In the present study, spin-orbit coupling and next-nearest-

*Also at Lyman Laboratory of Physics, Harvard University, Cambridge, MA 02138, USA.

neighbor hopping are neglected. We start from the gap equation [12], where the band dispersion law $\varepsilon_{\mathbf{k},\lambda}$ can be, in general, non-parabolic,

$$\begin{aligned} \Delta_\lambda(\mathbf{k}) &= -\frac{1}{(2\pi)^3} \int d\mathbf{k}' \Delta_\lambda(\mathbf{k}') \frac{\tanh \frac{\beta|\varepsilon_{\mathbf{k}',\lambda}|}{2}}{2|\varepsilon_{\mathbf{k}',\lambda}|} \\ &\times \frac{2}{\pi} \int_0^\infty d\Omega \frac{|\varepsilon_{\mathbf{k}',\lambda}| + |\varepsilon_{\mathbf{k},\lambda}|}{\Omega^2 + (|\varepsilon_{\mathbf{k}',\lambda}| + |\varepsilon_{\mathbf{k},\lambda}|)^2} \\ &\times V^R(\mathbf{k} - \mathbf{k}', i\Omega). \end{aligned} \quad (1)$$

Here $\beta = 1/(k_B T)$, λ is the index of a subband of the conduction band, $\Delta_\lambda(\mathbf{k})$ is the momentum-dependent gap function, $V^R(\mathbf{q}, i\Omega)$ is the matrix element of the effective electron-electron interaction in the polar crystal expressed through the total dielectric function of the electron-phonon system $\varepsilon^R(\mathbf{q}, i\Omega)$ in the Matsubara representation,

$$V^R(\mathbf{q}, i\Omega) = \frac{4\pi e^2}{q^2 \varepsilon^R(\mathbf{q}, i\Omega)} + V^{ac}(\mathbf{q}, i\Omega), \quad (2)$$

where $V^{ac}(\mathbf{q}, i\Omega)$ is the effective potential due to the acoustic deformation scattering from Ref. [13]. The acoustic-phonon scattering is not a dominating scattering channel in a strongly polar crystal, but this contribution is taken into account here for completeness.

Next, we use the density-of-states approximation using the density of states $\nu_\lambda(E)$ determined by the equation:

$$\frac{1}{4\pi^3} \int d\mathbf{k} F_\lambda(\varepsilon_{\mathbf{k},\lambda}) = \int_{\varepsilon_{\lambda,\min}}^{\varepsilon_{\lambda,\max}} F_\lambda(E) \nu_\lambda(E) dE, \quad (3)$$

where $\varepsilon_{\lambda,\max}$ and $\varepsilon_{\lambda,\min}$ are, respectively, the top and bottom energies in the λ -th subband, and $F_\lambda(E)$ is an arbitrary function of the energy.

In the density-of-states approximation, the band energy $\varepsilon_{\mathbf{k},\lambda}$ is modeled by a spherically symmetric band dispersion $\varepsilon_{k,\lambda}$. The model band dispersion is determined from the condition that the *density of states for $\varepsilon_{k,\lambda}$ is the same as the exact density of states* for a true energy band dispersion $\varepsilon_{\mathbf{k},\lambda}$. This condition results in the equation:

$$\int_{\varepsilon_{\lambda,\min}}^{\varepsilon_{\lambda}(k)} \nu_\lambda(E) dE = \frac{1}{3\pi^2} k^3. \quad (4)$$

The root of Eq. (4) determines the model band energy $\varepsilon_\lambda(k)$ for a given $\nu_\lambda(E)$ corresponding to the true band energy $\varepsilon_\lambda(\mathbf{k})$. In this approximation, the gap function depends on the energy $\varepsilon_{k,\lambda}$, and Eq. (1) is transformed to the equation:

$$\begin{aligned} \Delta_\lambda(\omega) &= -\int_{\varepsilon_{\lambda,\min}-\mu}^{\varepsilon_{\lambda,\max}-\mu} \frac{d\omega'}{2\omega'} \tanh\left(\frac{\beta\omega'}{2}\right) \\ &\times K_\lambda(\omega, \omega') \Delta_\lambda(\omega'), \end{aligned} \quad (5)$$

with the kernel function for non-parabolic bands:

$$\begin{aligned} K_\lambda(\omega, \omega') &= \frac{1}{2\pi} \frac{\nu_\lambda(\omega' + \mu)}{k_\lambda k'_\lambda} \int_{|k_\lambda - k'_\lambda|}^{k_\lambda + k'_\lambda} q dq \\ &\times \int_0^\infty d\Omega \frac{|\omega'| + |\omega|}{\Omega^2 + (|\omega'| + |\omega|)^2} V^R(q, i\Omega), \end{aligned} \quad (6)$$

where the energies ω, ω' are counted from the chemical potential μ , (which is close to the Fermi energy). The values of the momentum $k_\lambda \equiv p_\lambda(\omega)$ and $k'_\lambda \equiv p_\lambda(\omega')$ are expressed using the density of states:

$$p_\lambda(\omega) = \left(3\pi^2 \int_{\varepsilon_{\lambda,\min}}^{\mu+\omega} \nu_\lambda(E) dE \right)^{1/3}. \quad (7)$$

The total dielectric function entering the effective electron-electron interaction potential $V^R(q, i\Omega)$ is calculated within the random phase approximation (RPA). In RPA, the total dielectric function is a sum of the dielectric function of the lattice and the Lindhard polarization function $P^{(1)}(q, i\Omega)$ for electrons:

$$\varepsilon^R(q, i\Omega) = \varepsilon_\infty \prod_{j=1}^n \left(\frac{\Omega^2 + \omega_{L,j}^2(q)}{\Omega^2 + \omega_{T,j}^2(q)} \right) - \frac{4\pi e^2}{q^2} P^{(1)}(q, i\Omega). \quad (8)$$

The dielectric function of the lattice corresponds to the model of independent oscillators, where $\omega_{L,j}(q)$ and $\omega_{T,j}(q)$ are, respectively, LO- and TO-phonon frequencies, and ε_∞ is the high-frequency dielectric constant. Here, we assume the phonon dispersion law to be isotropic. The TO-mode frequencies have stronger q -dispersion than that for the LO-mode frequencies. Therefore we suggest only $\omega_{T,j}(q)$ to be q -dependent. Here, the TO-phonon dispersion is modeled by the expression,

$$\omega_{T,j}(q) = [\omega_{T,j}^2 + (\omega_{L,j}^2 - \omega_{T,j}^2) \sin^2(qa_0/\pi)]^{1/2}, \quad (9)$$

where a_0 is the lattice constant.

The Lindhard polarization function in the density-of-states approximation takes the form:

$$\begin{aligned} P^{(1)}(q, i\Omega) &= \frac{\pi^2}{q} \sum_\lambda \int_0^{\varepsilon_{\lambda,\max}} dE \frac{\nu_\lambda(E)}{k_\lambda(E)} f(E - \mu) \\ &\times \int_{\varepsilon_{\lambda,a}}^{\varepsilon_{\lambda,b}} dE' \frac{\nu_\lambda(E')}{k_\lambda(E')} \frac{E - E'}{\Omega^2 + (E - E')^2}. \end{aligned} \quad (10)$$

with the Fermi distribution functions $f(\varepsilon - \mu)$. The integration bounds are given by:

$$\begin{aligned} \varepsilon_{\lambda,a} &= \min(\varepsilon_\lambda(|p_\lambda(E) - q|), \varepsilon_{\lambda,\max}), \\ \varepsilon_{\lambda,b} &= \min(\varepsilon_\lambda(p_\lambda(E) + q), \varepsilon_{\lambda,\max}). \end{aligned} \quad (11)$$

Expanding (10) in powers of the momentum up to q^2 , we arrive at the expansion $(4\pi e^2/q^2) P^{(1)}(\mathbf{q}, i\Omega) = -\omega_p^2/\Omega^2 + O(q^2)$ with the plasma frequency,

$$\omega_p^2 = \sum_\lambda 4\pi e^2 n_\lambda \frac{k_{F,\lambda}}{\pi^2 \nu_\lambda(\mu)}. \quad (12)$$

where $k_{F,\lambda} = (3\pi^2 n_\lambda)^{1/3}$, and n_λ is the population of the λ -th subband. This long-wavelength limit allows us to introduce the effective mass parameter

$$m_\lambda \equiv \pi^2 \nu_\lambda(\mu) / k_{F,\lambda} \quad (13)$$

expressed through the density of states at the Fermi energy.

The long-wavelength expansion of $P^{(1)}(\mathbf{q}, i\Omega)$ gives a leading contribution to the effective potential. Therefore the polarization function $P^{(1)}(\mathbf{q}, i\Omega)$ calculated using the parabolic band approximation with the effective mass values given by (13), instead of those for the bottom of the conduction band, provides a good approximation for the effective interaction potential $V^R(q, i\Omega)$ in non-parabolic bands. Thus the major effect of the band non-parabolicity comes from the density of states entering the kernel function (6) rather than from the interaction potential.

CONCENTRATION DEPENDENT CRITICAL TEMPERATURES

In this section, we describe the calculated critical temperatures and the isotope effect in n -doped strontium titanate comparing the results with experimental data and discuss the relation of the present study to other works. The LO and TO phonon energies are extracted from the results of the density functional theory calculations using the Vienna ab initio simulation package (VASP) [24, 25]. All calculations were based on projector augmented wave pseudopotentials within the density functional theory. The PBEsol exchange-correlation functional [26] and a plane wave energy cutoff of 600 eV were used with a $12 \times 12 \times 12$ Monkhorst-Pack k -point mesh. The atomic positions were optimized until the forces were smaller than 0.01 eV/Å, and the phonon frequencies were computed using density functional perturbation theory with an energy accuracy of 10^{-8} eV.

The calculated and measured (shown in brackets) phonon frequencies are shown in Table I. We keep only those LO/TO pairs of frequencies which give a factor different from in the dielectric function and may be therefore observed. Even with this reduced set, the DFT calculation gives more frequencies than measured experimentally, because a significant ratio $\omega_{L,j}/\omega_{T,j}$ is necessary for detection.

The lowest-energy TO phonon mode, as measured in Ref. [27], exhibits concentration-dependent softening. We use interpolation to these experimental data for the lowest TO-phonon energy instead of the calculated value from Table 1 which does not account for softening. The high-frequency dielectric constant of SrTiO₃ is chosen according to Refs. [10, 28], $\epsilon_\infty = 5.1$. The acoustic deformation potential is used according to Ref. [29], $D = 4$ eV. In order to see the relative effect of the interaction

TABLE I: Energies of polar optical phonons in tetragonal SrTiO₃ at the Brillouin zone center

No. of the branch	$\hbar\omega_{L,j}$ (meV)	$\hbar\omega_{T,j}$ (meV)
1	103.62 (98.7 [30])	66.983 (67.6 [27])
2	61.521 (58.4 [30])	59.990
3	54.221	52.522
4	31.637	21.40 (21.8 [27])
5	18.305 (21.2 [30])	17.767
6	13.716	12.504 (11.0 [27])

with acoustic phonons we add also the transition temperature with $D = 0$.

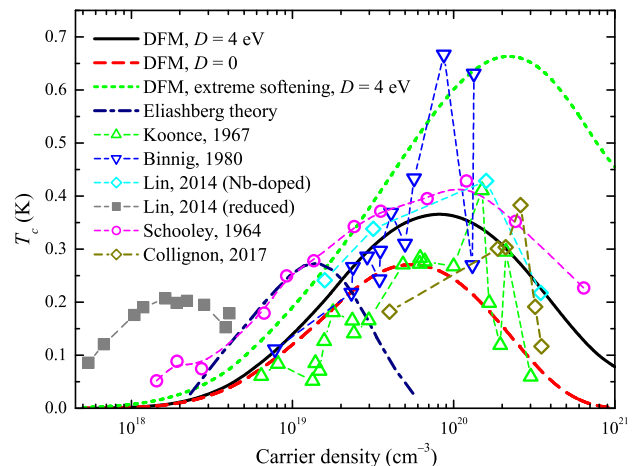


FIG. 1: *Solid and dashed curves*: critical temperature in n -doped SrTiO₃ as a function of the carrier density calculated within DFM using the density-of-states approximation for non-parabolic bands, with and without the acoustic-phonon contribution, respectively. *Dotted curve*: the same assuming the extreme softening of the lowest-energy TO-phonon mode. The calculated T_c is compared with experimental data of Refs. [1–5] (symbols). *Dot-dashed curve*: the result [10] of the Eliashberg theory.

The dispersion of the conduction band is described by the tight-binding analytic fit for the band Hamiltonian using the expressions and notations of Ref. [12]. We apply the values of the diagonal matrix elements t_δ, t_π from the tight-binding fit to the calculation performed using the GW method [31]: $t_\delta = 54.2$ meV, $t_\pi = 490.9$ meV. The conduction band splitting is a rather sensitive parameter, because it is relatively small with respect to diagonal matrix elements. As discussed in Ref. [10], the experimentally relevant values of the interband splitting are $\delta\epsilon_2 \approx 2$ meV and $\delta\epsilon_3 \approx 8$ meV. These values are obtained when using splitting parameters $\xi \approx 4.615$ meV and $d \approx 0.931$ meV.

It is observed in Ref. [8] that the polaronic effect [32] can substantially influence parameters of the superconducting state and critical temperatures. It is taken into account, scaling the bare-electron band energies $\epsilon_{\mathbf{k},\lambda}$ by

$\varepsilon_{\mathbf{k},\lambda}^{(pol)} = (m_\lambda/m_\lambda^*) \varepsilon_{\mathbf{k},\lambda}$, where the effective mass parameter m_λ is determined by (13). In the present calculation, we have used $\alpha_{eff} \approx 2.1$ [33], yielding $m_\lambda^*/m_\lambda \approx 1.35$.

In Fig. 1, we plot critical temperature in n -doped SrTiO₃ as a function of the carrier density calculated using the dielectric function method within the density-of-states approximation. The calculated critical temperatures are compared with experimental data of Refs. [1–5] and with the theoretical result for T_c predicted in Ref. [10] using the Eliashberg theory. As can be seen from Fig. 1, the calculated transition temperatures demonstrate good agreement with the experiments for concentrations $n \sim 5 \times 10^{18}$ to $5 \times 10^{20} \text{ cm}^{-3}$. A deviation between the present calculation and experiment does not exceed the deviations between different experiments. The latter is significant, because very small T_c may relatively strongly fluctuate in different experimental conditions. The present calculation does not match the experimental data of Refs. [1, 4] for low concentrations $n \lesssim 10^{18} \text{ cm}^{-3}$, where the calculated transition temperature decreases to small values with respect to these experimental results. The measured concentration dependence of T_c in this low-density range exhibits a separate dome. The superconductivity in this low-density regime may be attributed to another mechanism than the interaction with bulk phonons, for example, local modes proposed in Ref. [16]. The incorporation these local modes in the DFM is beyond the scope of the present work. There are also other pitfalls when trying to apply DFM at low concentrations: the electron-phonon interaction at low densities is less screened, so that the weak-coupling approximation may fail.

The non-parabolic dispersion in SrTiO₃ leads to a rapidly increasing density of states in the range of energies corresponding to Fermi energies for densities up to $n \sim 10^{20} \text{ cm}^{-3}$. This leads to better quantitative agreement of the calculated T_c with experimental data than in our preceding work [12]. The contribution of acoustic phonons results in an increase of T_c about 25% with a shift of the maximum of superconducting dome to higher densities. The transition temperature is also calculated assuming extremely strong softening of the lowest TO-phonon mode to a vanishingly small value. The result is not sensitive to this soft mode frequency when it is very small. The origin of this softening can be attributed, e. g., to quantum criticality [14]. In the present work we do not yet add the deformation potential interaction with the soft TO-phonon mode considered in Ref. [15]. Nevertheless, the softening of TO phonons influences T_c , because their frequencies enter the dielectric function and therefore enhance the Fröhlich interaction. As can be seen from Fig. 1, the softening leads to a substantial rise of T_c and to a shift of its maximum to a higher concentration.

Fig. 2 shows the calculated isotope effect in SrTiO₃ calculated using new band splitting parameters. The

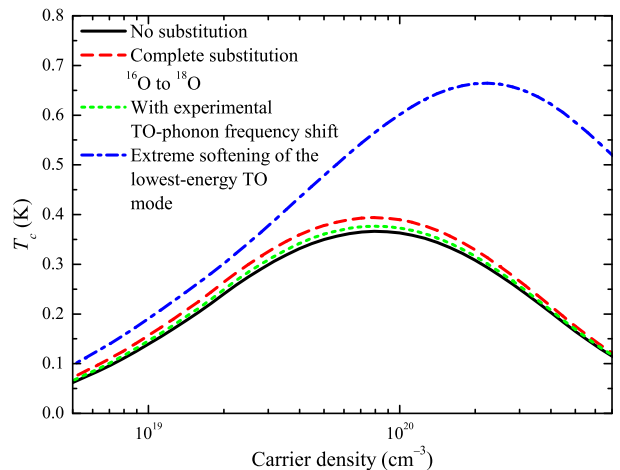


FIG. 2: Isotope effect for the critical temperature in n -doped SrTiO₃ calculated using the dielectric function method within the density-of-states approximation for non-parabolic bands. *Solid curve*: T_c without the isotope substitution. *Dashed curve*: T_c with the complete substitution $^{16}\text{O} \rightarrow ^{18}\text{O}$, and assuming proportional renormalization of all optical phonon frequencies. *Dotted curve*: T_c with the substitution corresponding to the experimental shift of the TO-phonon frequency. *Dot-dashed curve*: with the extreme softening of the lowest-energy TO mode.

curves in Fig. 2 correspond to the following conditions: (1) without the isotope substitution; (2) with the complete substitution $^{16}\text{O} \rightarrow ^{18}\text{O}$ without assuming appearance of the soft mode (the continuum approach [34] gives $\omega_{L(T),j} (^{18}\text{O}) / \omega_{L(T),j} (^{16}\text{O}) \approx 0.943$); (3) with the proportional change of phonon frequencies corresponding to the experimentally observed shift of the highest TO-phonon energy in Ref. [23]; (4) assuming extremely strong softening of the lowest TO-phonon mode as described above. The softening of the lowest-energy TO-phonon mode is in line with the observed increase of T_c due to the isotopic substitution $^{16}\text{O} \rightarrow ^{18}\text{O}$.

The softening leads to an increase of the effective Fröhlich coupling constant [which in the single-mode picture is proportional to $(1/\varepsilon_0 - 1/\varepsilon_\infty)$]. When $\varepsilon_0 \rightarrow \infty$, there is an enhancement of T_c (see discussions in [9, 19]). Also the phonon dispersion favors an increase of the transition temperature for relatively high concentrations $n \gtrsim 10^{19} \text{ cm}^{-3}$, where the plasmon contribution is not negligible [22]. The plasmon contribution enters T_c in a non-additive way, because the dielectric function within RPA (8) leads to a plasmon-phonon mixing. It is worth noting also that RPA goes beyond the frequently used plasmon-pole approximation, which results in damping of plasmon-phonon excitations.

CONCLUSIONS

In the present work, we have found a tractable extension of the dielectric function method for superconductivity to a non-parabolic band structure, considering the case of SrTiO₃. The DFM essentially includes retarded interactions and can be valid in a non-adiabatic regime, restricted by a weak-coupling approximation.

The density-of-states approach can represent an interest for practical use, because, first, it allows us to obtain an easily tractable gap equation. Second, it opens a way to calculate parameters of the superconducting state when the band dispersion is not precisely given, and only the density of states is known, e. g., from first-principle calculations or from experimental data.

The dielectric function method is capable to interpret superconductivity in strontium titanate without adjustment of material parameters, taking them from experimental data and microscopic calculations. All phonon branches existing in strontium titanate, as well as the phonon dispersions, are used for the numerical calculations. Both a non-parabolic band energy and the dispersion of phonons are essential for quantitative comparison with experiments. The dielectric function method predicts the sign of the observed unusual isotope effect in SrTiO₃ and a rise of the transition temperature due to softening of the lowest-energy TO-phonon mode. The resulting critical temperatures are in agreement with experiments in a range of concentrations $n \sim 5 \times 10^{18}$ to $5 \times 10^{20} \text{ cm}^{-3}$. The applicability of DFM at very low densities remains an open question. An inclusion of other interactions (e. g., deformation potential interaction with the soft TO-phonon mode [15] and the local phonons [16]) may improve results for transition temperatures.

The important feature of DFM is a prediction of superconductivity even in the case when the effective attraction between electrons does not exceed the Coulomb repulsion in the normal state. As a consequence, the obtained gap function exhibits a sign reversal near the Fermi surface, being in line with ab initio microscopic approaches [35]. This makes it interesting to treat DFM using the electron and phonon densities of states obtained from first principles.

This work has been supported by the joint FWO-FWF project POLOX (Grant No. I 2460-N36).

- [1] J. Schooley, W. Hosler, and M. L. Cohen, Phys. Rev. Lett. **12**, **474** (1964).
- [2] C. S. Koonce *et al.*, Phys. Rev. **163**, 380-390 (1967).
- [3] G. Binnig *et al.*, Phys. Rev. Lett. **45**, 1352-1355 (1980).
- [4] X. Lin *et al.*, Phys. Rev. Lett. **112**, 207002 (2014).
- [5] C. Collignon *et al.*, Phys. Rev. B **96**, 224506 (2017).
- [6] X. Lin *et al.*, Phys. Rev. B **92**, 174504 (2015).
- [7] C. W. Rischau *et al.*, Nat. Phys. **13**, 643 (2017).
- [8] A. G. Swartz *et al.*, PNAS **115**, 1475 (2018).
- [9] S. E. Rowley *et al.*, *arXiv:1801.08121*.
- [10] J. Ruhman and P. A. Lee, Phys. Rev. B **94**, 224515 (2016).
- [11] B. Rosenstein *et al.*, Phys. Rev. B **94**, 024505 (2016).
- [12] S. N. Klimin, J. Tempere, J. T. Devreese and D. der Marel, J. Sup. & Nov. Magn. **30**, 757 (2017).
- [13] S. N. Klimin, J. Tempere, J. T. Devreese and D. van der Marel, Phys. Rev. B **89**, 184514 (2014).
- [14] J. M. Edge *et al.*, Phys. Rev. Lett. **115**, 247002 (2015).
- [15] P. Wölfle and A. V. Balatsky, *arXiv:1803.06993*.
- [16] L. P. Gor'kov, J. Supercond. Nov. Magn. **30**, 845 (2017).
- [17] W. L. McMillan, Phys. Rev. **167**, 331 (1968).
- [18] D. A. Kirzhnits, E. G. Maksimov and D. I. Khomskii, J. Low Temp. Phys. **10**, 79-93 (1973).
- [19] L. V. Gurevich, A. I. Larkin, and Y. A. Firsov, Sov. Phys. Sol. State **4**, 131 (1962).
- [20] C. Collignon *et al.*, *arXiv:1804.07067*.
- [21] P. Morel and P. W. Anderson, Phys. Rev. **125**, 1263 (1962).
- [22] Y. Takada, J. Phys. Soc. Jpn. **45**, 786 (1978); **49**, 1267 (1980); **49**, 1713 (1980).
- [23] A. Stucky *et al.*, Sci. Rep. **6**, 37582 (2016).
- [24] G. Kresse and J. Hafner, Phys. Rev. B **47**, 558 (1993).
- [25] G. Kresse and J. Furthmüller, Phys. Rev. B **54**, 11169 (1996).
- [26] J. P. Perdew *et al.*, Phys. Rev. Lett. **100**, 136406 (2008); **102**, 039902 (2009).
- [27] J. L. M. van Mechelen *et al.*, Phys. Rev. Lett. **100**, 226403 (2008).
- [28] K. Kamarás *et al.*, J. Appl. Phys. **78**, 1235 (1995).
- [29] A. Janotti *et al.*, Appl. Phys. Lett. **100**, 262104 (2012).
- [30] F. Gervais *et al.*, Phys. Rev. B **47**, 8187 (1993).
- [31] Z. Ergönenc, B. Kim, P. Liu, G. Kresse, and C. Franchini, Phys. Rev. Materials **2**, 024601 (2018).
- [32] J. T. Devreese, *arXiv:1611.06122*.
- [33] J. T. Devreese *et al.*, Phys. Rev. B **81**, 125119 (2010).
- [34] M. Born and Huang Kun, *Dynamical Theory of Crystal Lattices* (Oxford University Press, 1954).
- [35] A. Sanna *et al.*, J. Phys. Soc. Jpn. **87**, 041012 (2018).